

# Transient Climate Sensitivity Depends on Base Climate Ocean Circulation

JIE HE

*Program in Atmospheric and Oceanic Sciences, Princeton University, and NOAA/Geophysical Fluid Dynamics Laboratory, Princeton, New Jersey*

MICHAEL WINTON AND GABRIEL VECCHI

*NOAA/Geophysical Fluid Dynamics Laboratory, Princeton, New Jersey*

LIWEI JIA

*Program in Atmospheric and Oceanic Sciences, Princeton University, and NOAA/Geophysical Fluid Dynamics Laboratory, Princeton, New Jersey*

MARIA RUGENSTEIN

*Institute for Atmospheric and Climate Science, ETH Zurich, Zurich, Switzerland*

(Manuscript received 9 August 2016, in final form 10 November 2016)

## ABSTRACT

There is large uncertainty in the simulation of transient climate sensitivity. This study aims to understand how such uncertainty is related to the simulation of the base climate by comparing two simulations with the same model but in which CO<sub>2</sub> is increased from either a preindustrial (1860) or a present-day (1990) control simulation. This allows different base climate ocean circulations that are representative of those in current climate models to be imposed upon a single model. As a result, the model projects different transient climate sensitivities that are comparable to the multimodel spread. The greater warming in the 1990-start run occurs primarily at high latitudes and particularly over regions of oceanic convection. In the 1990-start run, ocean overturning circulations are initially weaker and weaken less from CO<sub>2</sub> forcing. As a consequence, there are smaller reductions in the poleward ocean heat transport, leading to less tropical ocean heat storage and less moderated high-latitude surface warming. This process is evident in both hemispheres, with changes in the Atlantic meridional overturning circulation and the Antarctic Bottom Water formation dominating the warming differences in each hemisphere. The high-latitude warming in the 1990-start run is enhanced through albedo and cloud feedbacks, resulting in a smaller ocean heat uptake efficacy. The results highlight the importance of improving the base climate ocean circulation in order to provide a reasonable starting point for assessments of past climate change and the projection of future climate change.

## 1. Introduction

Climate models project a large range of surface warming from greenhouse gas forcing. As documented in the Intergovernmental Panel on Climate Change

Fifth Assessment Report (IPCC 2013), the transient climate response (TCR), defined as the global-mean surface temperature increase at year 70 of the 1pctCO<sub>2</sub> experiment, varies by more than a factor of 2. The large intermodel spread in transient warming emanates from not only the uncertainty in radiative forcing and atmospheric feedbacks (e.g., Hansen et al. 1984; Raper et al. 2002) but also the uncertainty in the rate of heat uptake by the ocean (Meehl et al. 2005; Stouffer et al. 2006b; Boé et al. 2009) and the efficacy of that heat uptake (Winton et al. 2010; Geoffroy et al. 2013).

A considerable amount of heat taken up by the ocean resides in the deep ocean (Gregory 2000; Raper et al. 2002; Kostov et al. 2014; Exarchou et al. 2015;

---

 Denotes content that is immediately available upon publication as open access.

---

 Supplemental information related to this paper is available at the Journals Online website: <http://dx.doi.org/10.1175/JCLI-D-16-0581.s1>.

---

Corresponding author e-mail: Jie He, [jie.he@noaa.gov](mailto:jie.he@noaa.gov)

DOI: 10.1175/JCLI-D-16-0581.1

© 2017 American Meteorological Society. For information regarding reuse of this content and general copyright information, consult the AMS Copyright Policy (<http://www.ametsoc.org/PUBSCopyrightPolicy>).

Rugenstein et al. 2016b), which is continuously filled by polar sinking water masses through the overturning circulation. As a result, the formation of deep water plays an important role in setting the ocean heat content and heat transport. In addition, during the transformation of surface water into dense sinking water, heat is released into the atmosphere, warming the surface climate at high latitudes (e.g., Winton 2003; Frierson et al. 2013). Changes in circulation, including the convection, are an important factor in the projection of transient warming (Rugenstein et al. 2013; Winton et al. 2014).

In the Northern Hemisphere, the sinking water is primarily formed in the Labrador Sea and Nordic seas and flows southward as part of the Atlantic meridional overturning circulation (AMOC). Models have shown that AMOC is important in regulating the pace of surface warming. The representation of AMOC varies greatly among models, contributing substantially to the uncertainty in transient warming (e.g., Gregory et al. 2005; IPCC 2007; Medhaug and Furevik 2011). Particularly, it has been shown that models with a stronger AMOC (Kostov et al. 2014) and a greater AMOC decline (Xie and Vallis 2012; Rugenstein et al. 2013; Winton et al. 2013, 2014) tend to project a slower transient warming.

In the Southern Hemisphere, convection primarily occurs in the Weddell and Ross Seas and along the Adélie coast to produce the Antarctic Bottom Water (AABW; Orsi et al. 1999), which fills the wide abyssal ocean. Observations between the 1980s and 2000s indicate a reduction of the AABW production and an associated warming of AABW, which accounts for most of the ocean heat uptake below 2000 m (Purkey and Johnson 2010, 2012, 2013). Unfortunately, this process cannot be accurately represented by climate models because of their large biases in Southern Ocean circulation (e.g., Russell et al. 2006; Downes et al. 2015). For example, the second phase of the Co-ordinated Ocean–Ice Reference Experiments shows a large spread in AABW formation from state-of-the-art climate models, ranging from 20 Sv ( $1 \text{ Sv} \equiv 10^6 \text{ m}^3 \text{ s}^{-1}$ ) to nonexistent (Farneti et al. 2015). The surface climatic impact of Southern Hemisphere convection is far less studied compared to its Northern Hemisphere counterpart, and the extent to which the simulation of AABW formation influences the global transient warming is yet to be determined.

To examine the impact of high-latitude convection on transient climate sensitivity, we compare two global warming experiments with the same model but initialized from different control runs: the one that starts from the preindustrial control run has a stronger initial AMOC and AABW production than the one that starts

from the present-day control run. Compared to the traditional approach of multimodel comparison, our approach is more effective at narrowing down the uncertainty to the simulation of the base climate as the responses in both experiments are governed by the same formula. This procedure can be used to determine the specific physical processes that need to be constrained for accurately projecting transient climate sensitivity.

For a more pragmatic purpose, this study also aims to examine whether the climate sensitivity observed or simulated from a low greenhouse gas condition can be directly applied to the contemporary climate change. For example, the preindustrial condition has been commonly used as the starting point for projecting TCR (e.g., Taylor et al. 2012). This is a convenient choice since the preindustrial climate can be assumed as an equilibrium state. However, because the base climate has changed substantially since the preindustrial era, it is unclear to what extent the preindustrial-based TCR can be used to inform about future warming. Our study will help clarify this matter by comparing the TCR simulated from preindustrial and present-day base climates.

## 2. Model simulation

The experiments used in this study are conducted with the GFDL Forecast-Oriented Low Ocean Resolution (FLOR) model. The FLOR model is built from the high-resolution Climate Model, version 2.5 (CM2.5; Delworth et al. 2012), by retaining its atmosphere and land resolution (approximately 50 km) and reducing its ocean and sea ice resolution from approximately  $1/4^\circ$  to approximately  $1^\circ$ . The combination of high-resolution atmosphere and relatively low-resolution ocean was originally designed for enhancing regional climate forecasting while maintaining a reasonable computational cost, as detailed by Vecchi et al. (2014). The version of the FLOR model used in this experiment is the one labeled FLOR-B01 in Vecchi et al. (2014) and Winton et al. (2014).

We conduct a preindustrial control run with 1860 atmospheric composition and a present-day control run with 1990 atmospheric composition. Both control runs are initialized with 1990 ocean and atmosphere observations that are assimilated into FLOR simulations (Zhang et al. 2007). Using such initialization is merely out of convenience since we do not have a spun-up FLOR model. We do not wish the model to mimic the observations; instead, we hope to obtain the model's climates under the 1860 and 1990 forcings for the respective perturbation runs. This normally requires a long spinup from each control run. As shown in Fig. S1 of the supplemental material, both control runs experience drastic adjustments in the first few decades and

remain relatively stable after 100 years. We perform two realizations of the 1pctCO<sub>2</sub> simulations branching off each control run after year 100. In the 1pctCO<sub>2</sub> simulations, CO<sub>2</sub> increases by 1% yr<sup>-1</sup> for 70 years until doubling is achieved and is held fixed afterward for another 170 years.

With the 100-yr spinup, models still experience climate drift during the 1pctCO<sub>2</sub> simulations: both the 1860 and 1990 control runs have a global-mean surface warming of about 0.15 K (100 yr)<sup>-1</sup>. This remains a caveat in the interpretation of our results. To minimize the impact of climate drift, we report all perturbation quantities as the difference between the corresponding years of the perturbed and control runs. Although the lack of sufficient spinup is not ideal, our goal is to study the impact of differences in the base climate ocean circulation, which are essentially not affected by the climate drift (see the supplemental material). We also conduct the 1pctCO<sub>2</sub> simulations with an additional 400-yr spinup, which yields consistent results (see the supplemental material).

### 3. Results

#### a. Overview of transient warming

The 1990-start run warms substantially more than the 1860-start run for the duration of the 1pctCO<sub>2</sub> simulations (Fig. 1). The warming difference is seen in both ensemble members and develops primarily during the CO<sub>2</sub> increasing period. The increase in global-mean surface temperature averaged over the last 50 years of the simulation (years 191–240) is 27% larger in the 1990-start run. The difference in TCR (estimated as the warming averaged over years 61–80) is 0.25 K, which is comparable to the CMIP5 multimodel standard deviation of 0.35 K (Gregory et al. 2015). Therefore, in this model, the projection of transient surface warming depends strongly on its starting point.

Figure 2 shows the spatial pattern of surface temperature changes. A polar amplification can be found in both simulations and is substantially stronger in the 1990-start run. In addition, there are large concentrated warming differences in high-latitude convective regions. In the 1860-start run, convective regions, particularly in the North Atlantic and the Weddell Sea, become colder (Fig. 2b), which is likely associated with a weakening of convection and a reduction in upward surface heat flux (Weaver et al. 2007; Newsom et al. 2016; Trossman et al. 2016). In the 1990-start run, the cooling is much weaker in the North Atlantic and absent in the Weddell Sea. These concentrated warming differences indicate an important

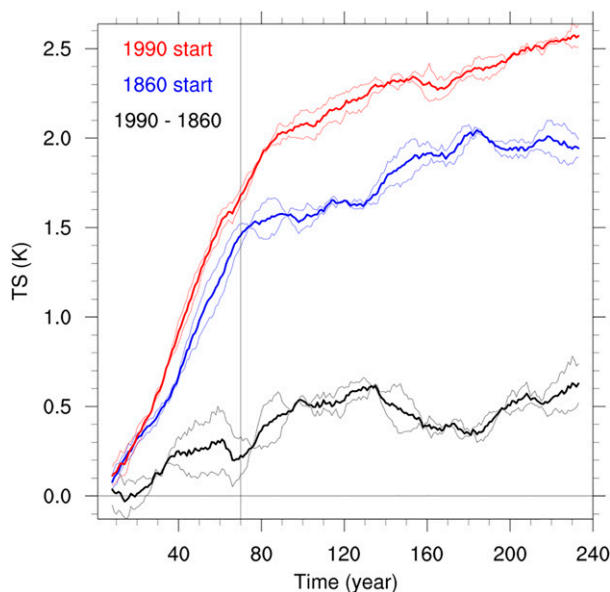


FIG. 1. Global-mean surface temperature (TS) change from the 1990-start (red) and 1860-start (blue) runs. Black lines show the difference between 1990-start and 1860-start runs. Thin lines are from the individual ensembles, whereas thick lines are the two ensemble mean. Data are plotted as the 15-yr running mean. The thin vertical line indicates the time of CO<sub>2</sub> doubling, after which CO<sub>2</sub> is held fixed.

connection to changes in high-latitude convection and overturning circulation, which will be examined in more detail later.

On a global scale, the transient surface warming can be thought of as being determined by three parameters: the equilibrium climate sensitivity (ECS), the ocean heat uptake efficiency, and the ocean heat uptake efficacy (Winton et al. 2010):

$$\delta T = \text{ECS} \frac{R}{R + \text{ECS} \varepsilon \gamma}, \quad (1)$$

where  $\delta T$  is the transient surface warming,  $R$  is the radiative forcing of doubled CO<sub>2</sub> (estimated as 3.5 W m<sup>-2</sup> for both simulations from radiation code),  $\varepsilon$  is the ocean heat uptake efficacy, and  $\gamma$  is the ocean heat uptake efficiency.

The ocean heat uptake efficiency is defined as

$$\gamma = \frac{N}{\delta T}, \quad (2)$$

where  $N$  is the net heat uptake, which is dominated by the ocean. The ocean heat uptake efficiency largely reflects the effectiveness of the deep ocean in absorbing the excess heat from radiative forcing, and a large efficiency acts to slow down surface warming (Gregory and Mitchell 1997; Raper et al. 2002).

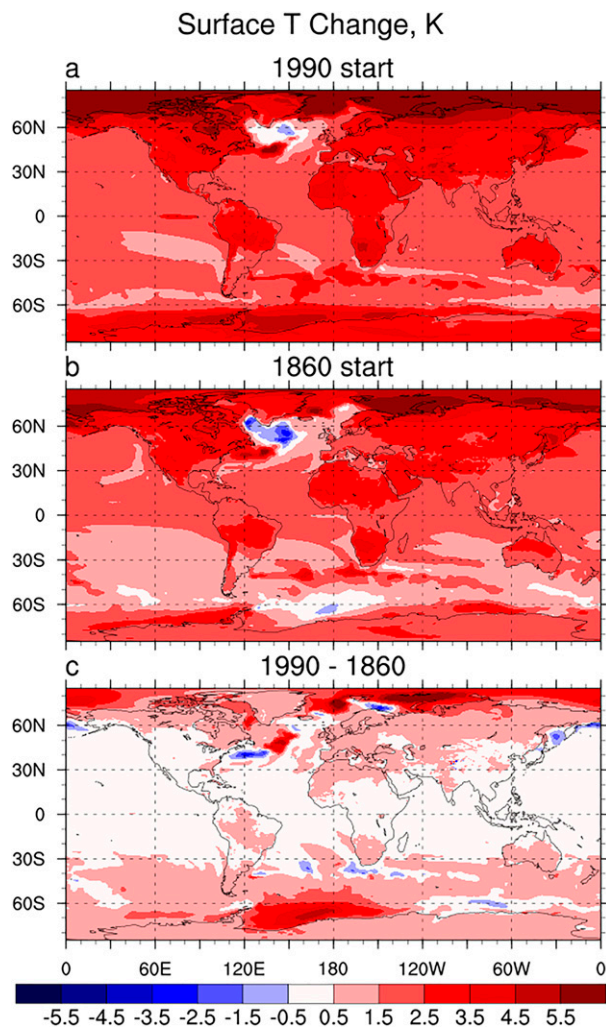


FIG. 2. Ensemble-mean surface temperature change (K) from (a) the 1990-start run, (b) the 1860-start run, and (c) the difference between the two. Changes are averaged over the last 50 years of the simulations.

The ocean heat uptake efficacy is defined as the global surface temperature impact of heat uptake relative to the impact of  $\text{CO}_2$  radiative forcing (Winton et al. 2010):

$$\varepsilon = \frac{R/\text{ECS}}{N/(\text{ECS} - \delta T)}. \quad (3)$$

It is essentially the ratio between the equilibrium radiative feedback and feedback of the ocean heat uptake. The efficacy reflects how ocean heat uptake affects the surface temperature through surface heat flux pattern-induced feedback response, and a large efficacy acts to slow down surface warming (e.g., Rugenstein et al. 2016a).

The ECS and the ocean heat uptake efficiency and efficacy are visualized in Fig. 3. A linear extrapolation of the surface temperature–top of the atmosphere

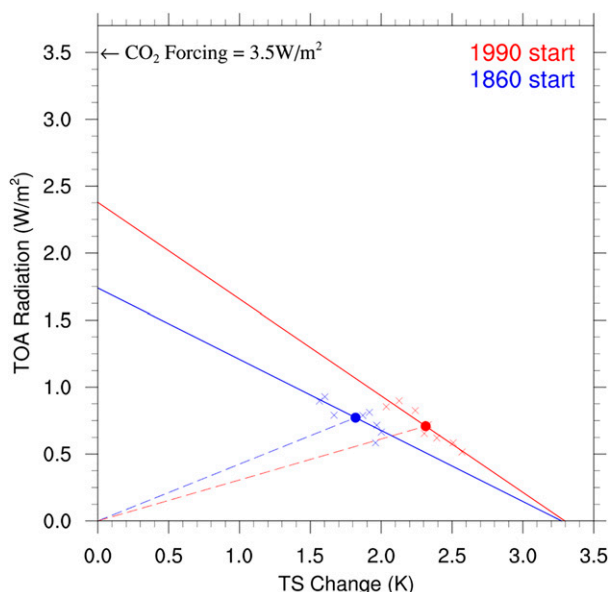


FIG. 3. Scatterplot of global-mean TOA radiation ( $\text{W m}^{-2}$ ) and surface temperature change (K) using 20-yr averages during the  $\text{CO}_2$  stabilization period (crosses). The dots show averages of the entire stabilization period. The solid lines fit the crosses, whereas the dashed lines connect the dots and the point (0, 0). The global-mean  $\text{CO}_2$  radiative forcing is shown on the y axis. Data are plotted for the two ensemble mean.

(TOA) radiation relationship following Gregory et al. (2004) indicates roughly equal ECS (3.27 K for the 1860 start and 3.30 K for the 1990 start) and equilibrium radiative feedbacks from the 1990-start and 1860-start runs.

The average ocean heat uptake efficiency for the  $\text{CO}_2$  stabilizing period is shown as the slope of the dashed line in Fig. 3, which connects the point of average surface temperature change and average TOA radiation change with point (0, 0). The efficiency is lower in the 1990-start run throughout the simulation and 28% lower during the  $\text{CO}_2$  stabilizing period. The heat uptake efficacy for the  $\text{CO}_2$  stabilizing period is shown as the ratio of the  $\text{CO}_2$  radiative forcing ( $3.5 \text{ W m}^{-2}$ ) to the y intercept of the solid lines in Fig. 3. The efficacy is 1.47 for the 1990-start run and 2.01 for the 1860-start run. Therefore, both the smaller heat uptake efficiency and the smaller efficacy in the 1990-start run account for its larger transient warming.

#### b. Ocean heat uptake and heat transport

The ocean heat uptake pattern is shown in Fig. 4. In the Northern Hemisphere, heat uptake primarily occurs in the North Atlantic convective regions (Figs. 4a,b) and is overall smaller in the 1990-start run (Fig. 4c). In the Southern Hemisphere, heat uptake is spread over most

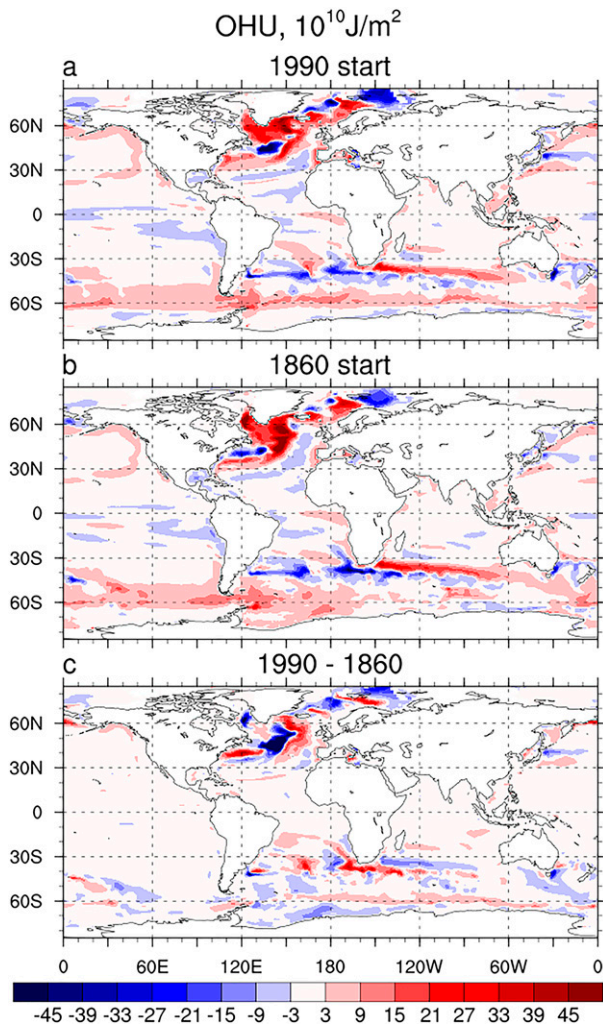


FIG. 4. Ensemble-mean surface ocean heat uptake (OHU;  $\text{J m}^{-2}$ ) calculated as changes in surface heat flux integrated over the entire 240 years of the simulation. Positive values indicate downward heat fluxes. The results are from the (a) 1990-start runs, (b) 1860-start runs, and (c) difference between the two. (Zonal integrals of the heat uptake for the high latitudes and the tropics are provided in Fig. 8.)

of the Southern Ocean. The most noticeable difference between the two runs is in the Weddell Sea, where only the 1860-start run shows positive heat uptake. Some quantitative differences can also be found throughout the Southern Ocean, with somewhat complex structures. Since high-latitude convection is often associated with heat being released into the atmosphere, the smaller heat uptake at convective regions in the 1990-start run indicates a smaller weakening of convection.

Figure 5 shows the climatology and changes of mixed layer depth, which is defined as the depth where the buoyancy difference with respect to the surface level is greater than or equal to  $0.0003 \text{ ms}^{-2}$  and can be used

as a measure of convection (Stouffer et al. 2006a). As shown in Figs. 5d–f, both the 1990-start and 1860-start runs project a general reduction in mixed layer depth, particularly at convective regions, indicating a weakening of convection. Consistent with the differences in heat uptake (Fig. 4c), the 1990-start run shows a smaller weakening of convection in the North Atlantic and the Weddell Sea (Figs. 5d–f). The smaller weakening is associated with the weaker initial convection, as the difference in the change (Fig. 5f) is almost exactly the opposite of the control climatology (Fig. 5c). This is consistent with previous studies (Gregory et al. 2005; Weaver et al. 2007; Newsom et al. 2016), which found that the weakening of convection largely depends on its initial strength.

To complement the high-latitude mixed layer depth, we present the zonally integrated meridional overturning circulation (MOC) in Fig. 6. The climatological MOC consists of an upper cell dominated by the AMOC and a lower cell dominated by the AABW formation (Figs. 6a,b). As shown in Fig. 6c, the 1990 control run has a weaker and shallower AMOC. Although the 1990 control run shows a stronger upwelling poleward of  $50^{\circ}\text{S}$ , it has a weaker lower cell as a result of its weaker convection in the Weddell Sea (Fig. 5c). In addition, the two control runs have little difference in the Antarctic Circumpolar Current transport (only 1.7% stronger in the 1990 control run), likely due to the cancellation between wind forcing and eddy adjustment (Meredith et al. 2012; Morrison and Hogg 2013). In the 1pctCO<sub>2</sub> simulations, both the AMOC and the AABW formation weaken. The weakening is smaller in the 1990-start run (Fig. 6f), which is again consistent with its weaker initial circulation (Fig. 6c).

To understand the connection between the circulation changes and transient sensitivity, we compare hemispheric surface warming, MOC weakening, and changes in poleward heat transport for the two 1pctCO<sub>2</sub> simulations (Fig. 7). The AMOC index is defined as the maximum streamfunction at  $40^{\circ}\text{N}$ , whereas the AABW index is defined as the minimum streamfunction multiplied by  $-1$  at  $69^{\circ}\text{S}$ . These latitudes are chosen because they exhibit the strongest AMOC and AABW formation, respectively, in the FLOR model's preindustrial control run; using a wider range of latitudes for the definition of the indices would yield similar results (not shown). Changes in the global poleward heat transport are calculated at  $40^{\circ}$  latitude. We treat this latitude as the lower bound of high-latitude regions mainly because AMOC is the strongest at  $40^{\circ}\text{N}$ , but our results are not very sensitive to this choice. Because subgrid-scale heat transport was not saved, we calculate poleward heat transport as the residual between ocean heat content

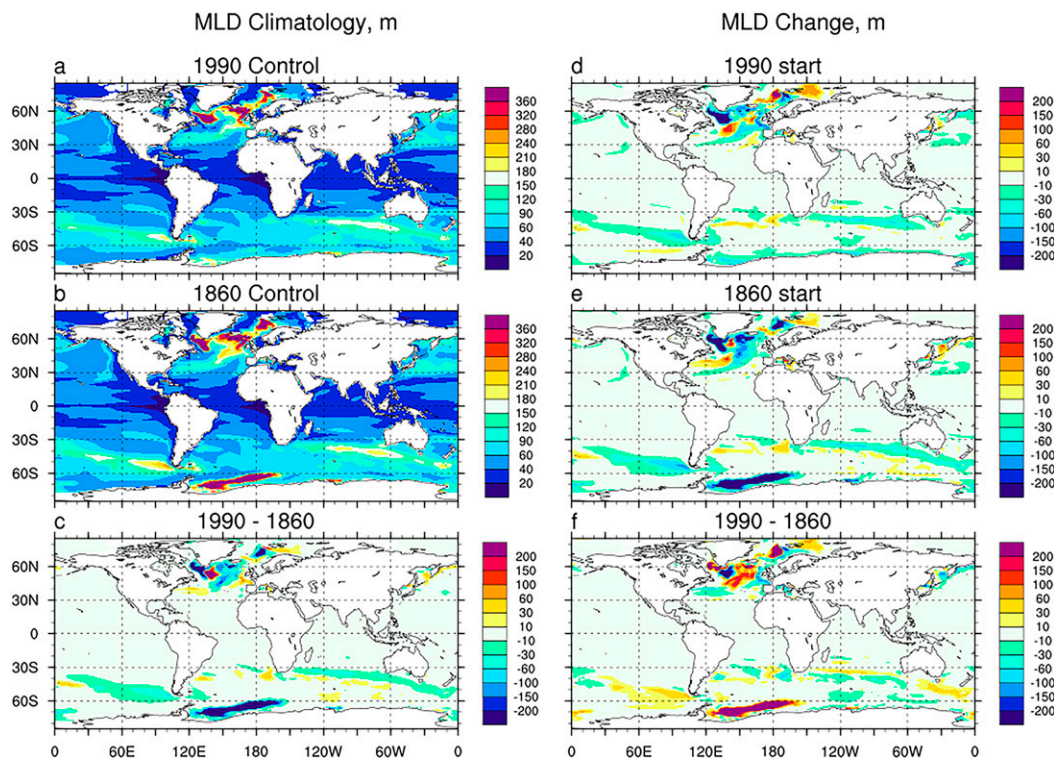


FIG. 5. Ensemble-mean mixed layer depth (MLD) (a)–(c) climatology and (d)–(f) change (m). Climatology is calculated as the 240-yr average from the control runs, whereas change is calculated as the average over the last 50 years of the perturbed runs. Results are from the (a),(b) 1990-start runs (d),(e) 1860-start runs, and (c),(f) difference between the two.

tendency and changes in surface heat flux averaged poleward of  $40^{\circ}$ . We note that this is not an exact calculation because we did not account for the varying thickness of the top and bottom grid cells when obtaining the ocean heat storage. We will further discuss this caveat in section 3c.

As shown in Figs. 7a and 7d, the Northern and Southern Hemispheres (primarily at high latitudes, Fig. 2c) contribute about equally to the global difference in transient warming. For the Northern Hemisphere, the AMOC weakens initially and stabilizes around year 100 when the  $\text{CO}_2$  concentration is stabilized (Fig. 7b). The AMOC in the 1860-start run is initially 4 Sv stronger and eventually reaches similar amplitude as that in the 1990-start run, which means a greater weakening in the 1860-start run. As a result, it has a larger reduction in the poleward ocean heat transport (Fig. 7c), leading to a more moderated northern high-latitude warming (Figs. 7a and 2c). In addition, the temporal variability of Northern Hemisphere warming and heat transport change is generally consistent with the variability of AMOC change (black lines in Fig. 7). For example, during the first 35 years, the 1860-start run undergoes a faster AMOC weakening; correspondingly, it shows a

faster reduction in poleward ocean heat transport and a slower warming. During years 130–160, the AMOC recovers in the 1860-start run, leading to a recovery in poleward heat transport and an accelerated Northern Hemisphere warming, which does not occur in the 1990-start run. These results are consistent with Rugenstein et al. (2013), who found a similar relationship between AMOC weakening and high-latitude warming in two pairs of closely related GFDL models.

In the Southern Hemisphere, the warming difference shows a steady development during the first 140 years (Fig. 7d), similar to the difference in AABW decline (Fig. 7e). After year 140, the AABW formation stabilizes at similar amplitudes and the separation in surface warming slows down. This relationship is consistent with the fact that much of the Southern Hemisphere warming difference is concentrated over the Weddell Sea (Fig. 2c), where the 1860-start run shows a reduction in upward surface heat flux (Fig. 4b) and a surface cooling (Fig. 2b).

The cause and effect in the concurrence of AABW weakening and reduced surface heat loss are yet to be determined, and it is likely that they assist in each other's development. That is, the reduced surface heat

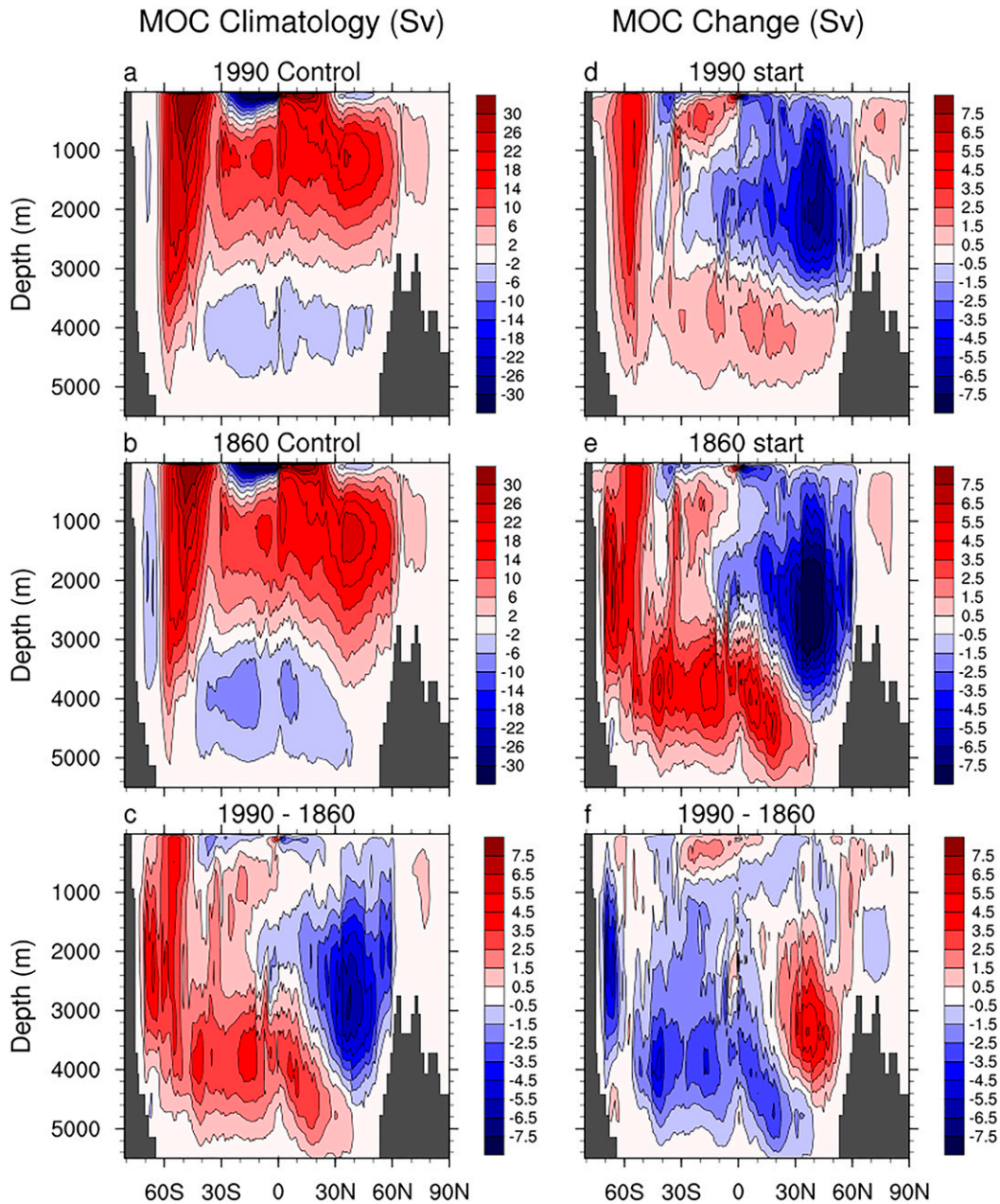


FIG. 6. As in Fig. 5, but for the zonally integrated streamfunction.

loss could weaken convection through buoyancy forcing (Newsom et al. 2016), whereas the weakening of the overturning circulation could also reduce the upward heat release by decreasing poleward ocean heat transport, similar to the process in the northern high latitude (e.g., Winton et al. 2013; Rugenstein et al. 2013). Indeed, the Southern Hemisphere poleward heat transport shows a greater reduction in the 1860-start run. This is consistent with its greater weakening of the lower cell, which is the dominant difference in Southern

Hemisphere MOC (Fig. 6f). Differences in the upper cell, albeit smaller, may also be important, considering the much larger temperature gradient in the upper ocean. Further studies are needed to understand these processes.

### c. Global ocean heat budget

To summarize the relationship between ocean heat transport and transient warming, we present the ocean heat budget for the northern and southern high latitudes

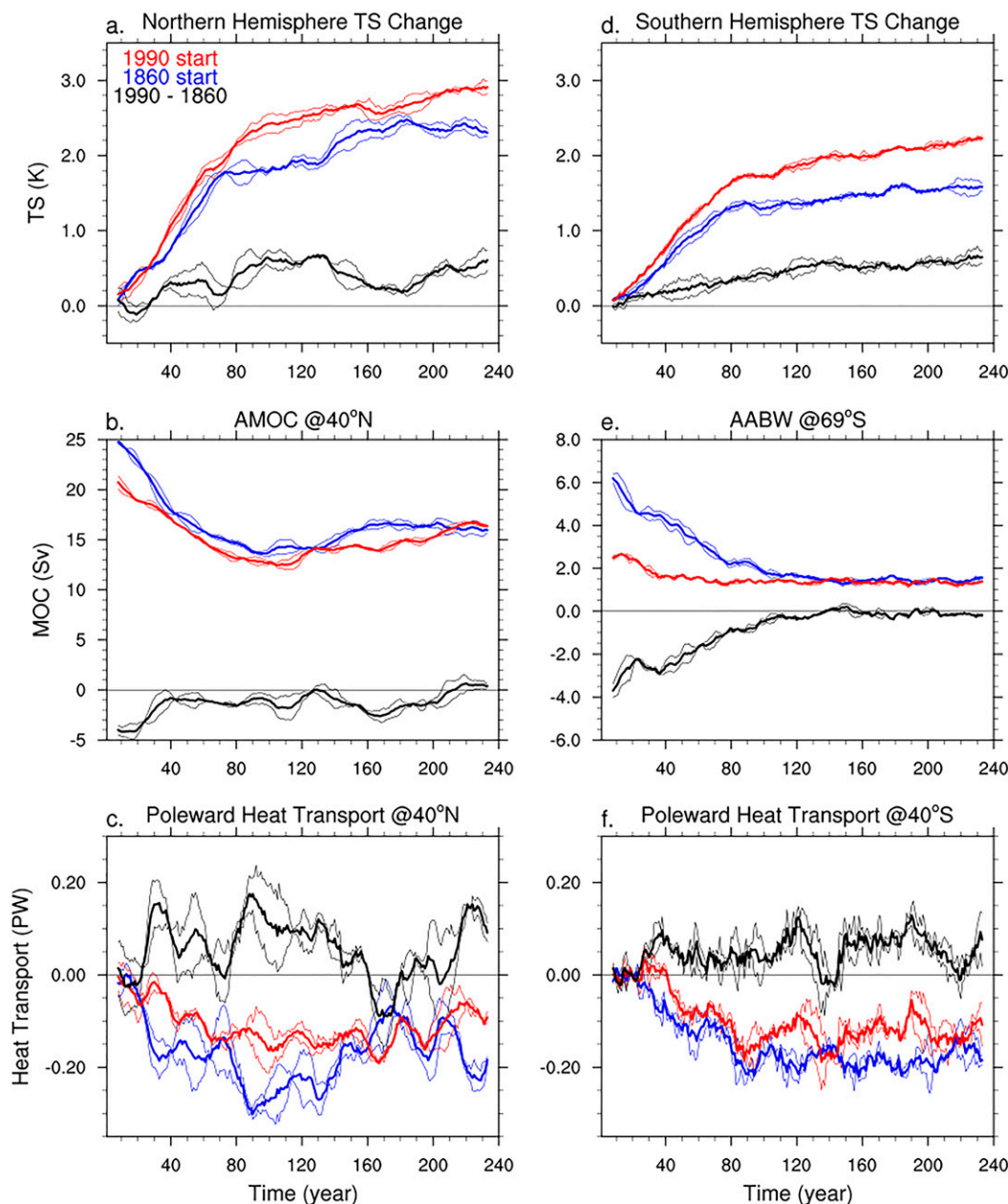


FIG. 7. (a),(d) Time series of hemispheric surface warming, (b) AMOC, (e) AABW, and (c),(f) changes in the zonally integrated poleward global ocean heat transport at  $40^{\circ}\text{N}$  and  $40^{\circ}\text{S}$ , respectively. AMOC and AABW are calculated at  $40^{\circ}\text{N}$  and  $69^{\circ}\text{S}$ , respectively, and their control run anomalies are removed to reduce the impact of model drift. Ocean heat transport is calculated indirectly as the difference between ocean heat storage tendency and changes in surface heat flux. Thin lines are from the individual ensembles, whereas thick lines are the two ensemble mean. Data are plotted as 15-yr running mean.

and the tropics (Fig. 8). The three regions are bounded by the  $40^{\circ}$  latitude. For each region, we calculate changes in surface heat flux and ocean heat storage tendency directly from the model output and estimate changes in ocean heat transport as the difference between the two. Because we did not account for the varying thickness of the top and bottom grid cells when

calculating the ocean heat storage, there is a small difference (less than 2%) between the global surface heat flux change and ocean heat storage tendency. As indicated by the colored arrows, the ocean circulation transports heat poleward from the tropics and eventually releases it into the atmosphere at high latitudes. As the circulation weakens, the poleward heat transport is

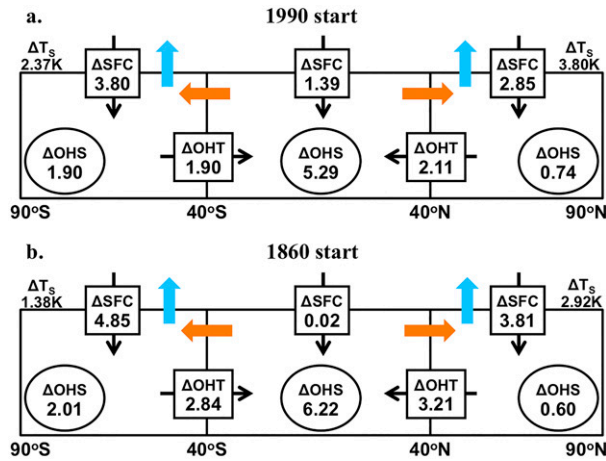


FIG. 8. Ensemble-mean changes in surface heat flux (SFC), changes in meridional ocean heat transport (OHT), and ocean heat storage tendency (OHS) averaged over the entire simulation for the (a) 1990-start run and (b) 1860-start run. Variables are integrated over three climate zones, which are bounded by the 40° latitude, and divided by the global earth surface area. Unit is  $0.1 \text{ W m}^{-2}$ . The OHT change ( $\Delta\text{OHT}$ ) is calculated as the difference between  $\Delta\text{OHS}$  and  $\Delta\text{SFC}$  in the high-latitude zones. Black arrows indicate the direction of the heat flux changes. Surface temperature changes poleward of 40° averaged over the last 50 years of the simulations are also shown. Blue and orange arrows indicate the direction of the climatological SFC and OHT, respectively.

reduced, and less heat is released into the high-latitude atmosphere, thereby moderating high-latitude warming.

In the 1860-start run, the circulation is initially stronger and weakens more, leading to a larger reduction in poleward heat transport and a slower high-latitude warming. Correspondingly, there is more heat uptake at high latitudes. Most of the high-latitude heat uptake is stored in the tropics through the reduced poleward heat transport. The large high-latitude heat uptake relative to the tropics in the 1860-start run is also consistent with its large heat uptake efficacy, as studies have shown that the cooling impact of heat uptake is more effective at high latitudes than the tropics (Kang and Xie 2014; Rose et al. 2014).

#### d. Heat uptake efficacy and transient feedback

The greater high-latitude warming of the 1990-start run induced by its smaller reduction in poleward heat transport can be further amplified by atmospheric radiative feedbacks, as indicated by its smaller ocean heat uptake efficacy (Fig. 3). To determine the source of the efficacy difference, we calculate the transient radiative feedbacks for the  $\text{CO}_2$  stabilization period using the GFDL model for radiative kernels (Soden et al. 2008).

TABLE 1. Transient radiative feedbacks ( $\text{W m}^{-2} \text{K}^{-1}$ ) during the  $\text{CO}_2$  stabilization period calculated using radiative kernels. Corrected total feedback using the average TOA radiation and surface temperature change during the  $\text{CO}_2$  stabilization period and corrected cloud feedback using the corrected total feedback, while assuming the accuracy of kernel-based temperature  $T$ , water vapor (WV), and albedo feedbacks, are shown in the parentheses.

	$T + \text{WV}$	Albedo	Cloud	Total
1990 start	-2.00	0.28	0.61 (0.52)	-1.12 (-1.21)
1860 start	-2.00	0.23	0.51 (0.28)	-1.27 (-1.50)
1990 minus 1860 start	0.00	0.05	0.10 (0.24)	0.15 (0.29)

As shown in Table 1, the kernel-based transient radiative feedback is  $0.15 \text{ W m}^{-2} \text{K}^{-1}$  higher in the 1990-start run. This is an underestimation compared to those directly calculated using the average TOA radiation and surface temperature change, which yields a  $0.29 \text{ W m}^{-2} \text{K}^{-1}$  higher feedback in the 1990-start run. The disparity is likely caused by the uncertainty in the cloud radiative kernels, but the uncertainty in other radiative kernels and the  $\text{CO}_2$  radiative forcing may also contribute. Here, we assume the accuracy of the kernel-based temperature, water vapor, and albedo feedbacks and show the corrected cloud feedback and total feedback in the parentheses.

The higher transient feedback in the 1990-start run is partly associated with the higher albedo feedback and mainly with the greater cloud feedback. This is consistent with previous studies (Winton 2003; Rose et al. 2014; Trossman et al. 2016; Zhang et al. 2010), which showed that cloud feedback is the dominant radiative feedback mechanism that responds to ocean circulation change. The larger cloud feedback in the 1990-start run is primarily associated with its greater reduction in high-latitude low clouds (figures not shown). The greater low-cloud reduction is possibly caused by the larger decrease in high-latitude tropospheric stability (Winton 2003) associated with the higher polar amplification (Fig. 2).

## 4. Conclusions and discussion

In this study, we compared the transient warming in the 1pct $\text{CO}_2$  simulations initialized from an 1860 control run and a 1990 control run. Previous studies showed that TCR could be sensitive to the differences in initial conditions that result from internal variability and model drift (Sen Gupta et al. 2012; Liang et al. 2013a,b). The main objective of this study is to understand the specific model biases in the simulation of base climate ocean circulation that potentially degrade the projection of transient climate sensitivity.

The global-mean surface temperature increases substantially faster in the 1990-start run compared to the 1860-start run. The greater transient warming is attributed to the smaller ocean heat uptake efficiency and smaller ocean heat uptake efficacy. In the 1990-start run, the overturning circulations are initially weaker and thereby weaken less from CO<sub>2</sub> forcing. As a result, there is a smaller reduction in poleward heat transport leading to a faster high-latitude warming. The warming disparity is further amplified partially through albedo feedback and primarily through cloud feedback.

The initial circulation difference in the two simulations is dominated by their differences in the AMOC and the AABW formation. The stronger initial AMOC and AABW formation in the 1860-start run allows a larger weakening, which leads to a surface cooling in the convective regions and a moderated high-latitude warming in the corresponding hemispheres. This cooling effect of ocean circulation is much less appreciable in the 1990-start run since the circulation is already substantially weakened at the beginning of the simulation. One may think of the slower transient warming in the 1860-start run as being delayed by the weakening of circulation. However, such “delay” becomes less effective as the climate continues to warm.

Since most climate models project a weakening of the overturning circulation, their TCRs, which are often simulated from a preindustrial starting point, are affected by the delay and should be smaller than future warming under the same radiative forcing. Other factors, such as ocean thermal stratification and the increase in radiative feedbacks, may also contribute to the delay (e.g., Gregory et al. 2015). Although we have used the 1860 and 1990 control runs to illustrate the importance of the starting point, the ideal initialization for projecting future TCR should be taken from the present-day simulation, in which warming is already under way, instead of a control run, which would induce a cold-start retardation (Hasselmann et al. 1993).

Although the initial circulation differences in our simulations were artificially created by modifying the radiative forcing, they are well within the intermodel spread (Gregory et al. 2005; Farneti et al. 2015). These circulation differences, even imposed upon the same model, would result in differences in TCR that are comparable to the intermodel spread. This suggests that biases in the base climate ocean circulation, particularly AMOC and AABW, need to be constrained for accurate projections of transient warming. The importance of AMOC has been widely addressed (e.g., Meehl et al. 2005; Rugenstein et al. 2013; Kostov et al. 2014). In comparison, the climatic impact of AABW formation has received far less attention, partially because it is too

weak or even nonexistent in many models (Frölicher et al. 2015; Farneti et al. 2015; Rugenstein et al. 2016b). In addition, the lack of observation on the strength of Antarctic convection makes model improvement rather difficult. However, the Weddell Sea polynya of the 1970s gave evidence of deep convection in the historical period. De Lavergne et al. (2014) found that almost one-third of the CMIP5 climate models do not have such convection in their preindustrial simulations. Our results suggest that this might result in an overestimation of Southern Ocean warming in these models. A recent study (Newsom et al. 2016) showed that the AABW formation is substantially stronger when the resolution of ocean model increases from 1° to 0.1°. Such studies are encouraged for better understanding the uncertainty in the simulation of AABW.

*Acknowledgments.* We thank Jonathan Gregory and Isaac Held for useful discussions and Thomas Delworth for the internal review at Geophysical Fluid Dynamics Laboratory. Thanks also go to Brian Soden and Eui-Seok Chung for providing radiative kernels. Jie He is supported by the visiting research scientist program at the Program in Atmospheric and Oceanic Sciences, Princeton University.

#### REFERENCES

- Boé, J., A. Hall, and X. Qu, 2009: Deep ocean heat uptake as a major source of spread in transient climate change simulations. *Geophys. Res. Lett.*, **36**, L22701, doi:10.1029/2009GL040845.
- De Lavergne, C., J. B. Palter, E. D. Galbraith, R. Bernardello, and I. Marinov, 2014: Cessation of deep convection in the open Southern Ocean under anthropogenic climate change. *Nat. Climate Change*, **4**, 278–282, doi:10.1038/nclimate2132.
- Delworth, T. L., and Coauthors, 2012: Simulated climate and climate change in the GFDL CM2.5 high-resolution coupled climate model. *J. Climate*, **25**, 2755–2781, doi:10.1175/JCLI-D-11-00316.1.
- Downes, S. M., and Coauthors, 2015: An assessment of Southern Ocean water masses and sea ice during 1988–2007 in a suite of interannual CORE-II simulations. *Ocean Modell.*, **94**, 67–94, doi:10.1016/j.ocemod.2015.07.022.
- Exarchou, E., T. Kuhlbrodt, J. M. Gregory, and R. S. Smith, 2015: Ocean heat uptake processes: A model intercomparison. *J. Climate*, **28**, 887–908, doi:10.1175/JCLI-D-14-00235.1.
- Farneti, R., and Coauthors, 2015: An assessment of Antarctic Circumpolar Current and Southern Ocean meridional overturning circulation during 1958–2007 in a suite of interannual CORE-II simulations. *Ocean Modell.*, **93**, 84–120, doi:10.1016/j.ocemod.2015.07.009.
- Frierson, D. M. W., and Coauthors, 2013: Contribution of ocean overturning circulation to tropical rainfall peak in the Northern Hemisphere. *Nat. Geosci.*, **6**, 940–944, doi:10.1038/ngeo1987.
- Frölicher, T. L., J. L. Sarmiento, D. J. Paynter, J. P. Dunne, J. P. Krasting, and M. Winton, 2015: Dominance of the Southern

- Ocean in anthropogenic carbon and heat uptake in CMIP5 models. *J. Climate*, **28**, 862–886, doi:10.1175/JCLI-D-14-00117.1.
- Geoffroy, O., D. Saint-Martin, G. Bellon, A. Voldoire, D. J. L. Olivie, and S. Tytca, 2013: Transient climate response in a two-layer energy-balance model. Part II: Representation of the efficacy of deep-ocean heat uptake and validation for CMIP5 AOGCMs. *J. Climate*, **26**, 1859–1876, doi:10.1175/JCLI-D-12-00196.1.
- Gregory, J. M., 2000: Vertical heat transports in the ocean and their effect on time-dependent climate change. *Climate Dyn.*, **16**, 501–515, doi:10.1007/s003820000059.
- , and J. F. B. Mitchell, 1997: The climate response to CO<sub>2</sub> of the Hadley Centre coupled AOGCM with and without flux adjustment. *Geophys. Res. Lett.*, **24**, 1943–1946, doi:10.1029/97GL01930.
- , and Coauthors, 2004: A new method for diagnosing radiative forcing and climate sensitivity. *Geophys. Res. Lett.*, **31**, L03205, doi:10.1029/2003GL018747.
- , and Coauthors, 2005: A model intercomparison of changes in the Atlantic thermohaline circulation in response to increasing atmospheric CO<sub>2</sub> concentration. *Geophys. Res. Lett.*, **32**, L12703, doi:10.1029/2005GL023209.
- , T. Andrews, and P. Good, 2015: The inconstancy of the transient climate response parameter under increasing CO<sub>2</sub>. *Philos. Trans. Roy. Soc. London*, **373A**, 20140417, doi:10.1098/rsta.2014.0417.
- Hansen, J., A. Lacis, D. Rind, G. Russell, P. Stone, I. Fung, R. Ruedy, and J. Lerner, 1984: Climate sensitivity: Analysis of feedback mechanisms. *Climate Processes and Climate Sensitivity*, *Geophys. Monogr.*, Vol. 29, Amer. Geophys. Union, 130–163, doi:10.1029/GM029p0130.
- Hasselmann, K., R. Sausen, E. Maier-Reimer, and R. Voss, 1993: On the cold start problem in transient simulations with coupled atmosphere–ocean models. *Climate Dyn.*, **9**, 53–61, doi:10.1007/BF00210008.
- IPCC, 2007: *Climate Change 2007: The Physical Science Basis*. Cambridge University Press, 996 pp.
- , 2013: *Climate Change 2013: The Physical Science Basis*. Cambridge University Press, 1535 pp., doi:10.1017/CBO9781107415324.
- Kang, S. M., and S.-P. Xie, 2014: Dependence of climate response on meridional structure of external thermal forcing. *J. Climate*, **27**, 5593–5600, doi:10.1175/JCLI-D-13-00622.1.
- Kostov, Y., K. C. Armour, and J. Marshall, 2014: Impact of the Atlantic meridional overturning circulation on ocean heat storage and transient climate change. *Geophys. Res. Lett.*, **41**, 2108–2116, doi:10.1002/2013GL058998.
- Liang, M.-C., L.-C. Lin, K.-K. Tung, Y. L. Yung, and S. Sun, 2013a: Transient climate response in coupled atmospheric–ocean general circulation models. *J. Atmos. Sci.*, **70**, 1291–1296, doi:10.1175/JAS-D-12-0338.1.
- , —, —, —, and —, 2013b: Impact of climate drift on twenty-first-century projection in a coupled atmospheric–ocean general circulation model. *J. Atmos. Sci.*, **70**, 3321–3327, doi:10.1175/JAS-D-13-0149.1.
- Medhaug, I., and T. Furevik, 2011: North Atlantic 20th century multidecadal variability in coupled climate models: Sea surface temperature and ocean overturning circulation. *Ocean Sci.*, **7**, 389–404, doi:10.5194/os-7-389-2011.
- Meehl, G. A., W. M. Washington, W. D. Collins, J. M. Arblaster, A. Hu, L. E. Buja, W. G. Strand, and H. Teng, 2005: How much more global warming and sea level rise? *Science*, **307**, 1769–1772, doi:10.1126/science.1106663.
- Meredith, M. P., A. C. Naveira Garabato, A. M. Hogg, and R. Farneti, 2012: Sensitivity of the overturning circulation in the Southern Ocean to decadal changes in wind forcing. *J. Climate*, **25**, 99–110, doi:10.1175/2011JCLI4204.1.
- Morrison, A. K., and A. M. Hogg, 2013: On the relationship between Southern Ocean overturning and ACC transport. *J. Phys. Oceanogr.*, **43**, 140–148, doi:10.1175/JPO-D-12-057.1.
- Newsom, E. R., C. M. Bitz, F. O. Bryan, R. Abernathey, and P. R. Gent, 2016: Southern Ocean deep circulation and heat uptake in a high-resolution climate model. *J. Climate*, **29**, 2597–2619, doi:10.1175/JCLI-D-15-0513.1.
- Orsi, A. H., G. C. Johnson, and J. L. Bullister, 1999: Circulation, mixing, and production of Antarctic Bottom Water. *Prog. Oceanogr.*, **43**, 55–109, doi:10.1016/S0079-6611(99)00004-X.
- Purkey, S. G., and G. C. Johnson, 2010: Warming of global abyssal and deep Southern Ocean waters between the 1990s and 2000s: Contributions to global heat and sea level rise budgets. *J. Climate*, **23**, 6336–6351, doi:10.1175/2010JCLI3682.1.
- , and —, 2012: Global contraction of Antarctic Bottom Water between the 1980s and 2000s. *J. Climate*, **25**, 5830–5844, doi:10.1175/JCLI-D-11-00612.1.
- , and —, 2013: Antarctic Bottom Water warming and freshening: Contributions to sea level rise, ocean freshwater budgets, and global heat gain. *J. Climate*, **26**, 6105–6122, doi:10.1175/JCLI-D-12-00834.1.
- Raper, S. C. B., J. M. Gregory, and R. J. Stouffer, 2002: The role of climate sensitivity and ocean heat uptake on AOGCM transient temperature response. *J. Climate*, **15**, 124–130, doi:10.1175/1520-0442(2002)015<0124:TROCSA>2.0.CO;2.
- Rose, B. E. J., K. C. Armour, D. S. Battisti, N. Feldl, and D. D. B. Koll, 2014: The dependence of transient climate sensitivity and radiative feedbacks on the spatial pattern of ocean heat uptake. *Geophys. Res. Lett.*, **41**, 1071–1078, doi:10.1002/2013GL058955.
- Rugenstein, M. A. A., M. Winton, R. J. Stouffer, S. M. Griffies, and R. Hallberg, 2013: Northern high-latitude heat budget decomposition and transient warming. *J. Climate*, **26**, 609–621, doi:10.1175/JCLI-D-11-00695.1.
- , K. Caldeira, and R. Knutti, 2016a: Dependence of global radiative feedbacks on evolving patterns of surface heat fluxes. *Geophys. Res. Lett.*, **43**, 9877–9885, doi:10.1002/2016GL070907.
- , J. Sedláček, and R. Knutti, 2016b: Nonlinearities in patterns of long-term ocean warming. *Geophys. Res. Lett.*, **43**, 3380–3388, doi:10.1002/2016GL068041.
- Russell, J. L., R. J. Stouffer, and K. W. Dixon, 2006: Intercomparison of the Southern Ocean circulations in IPCC coupled model control simulations. *J. Climate*, **19**, 4560–4575, doi:10.1175/JCLI3869.1.
- Sen Gupta, A., L. C. Muir, J. N. Brown, S. J. Phipps, P. J. Durack, D. Monselesan, and S. E. Wijffels, 2012: Climate drift in the CMIP3 models. *J. Climate*, **25**, 4621–4640, doi:10.1175/JCLI-D-11-00312.1.
- Soden, B. J., I. M. Held, R. Colman, K. M. Shell, J. T. Kiehl, and C. A. Shields, 2008: Quantifying climate feedbacks using radiative kernels. *J. Climate*, **21**, 3504–3520, doi:10.1175/2007JCLI2110.1.
- Stouffer, R. J., and Coauthors, 2006a: GFDL’s CM2 global coupled climate models. Part IV: Idealized climate response. *J. Climate*, **19**, 723–740, doi:10.1175/JCLI3632.1.
- , J. Russell, and M. J. Spelman, 2006b: Importance of oceanic heat uptake in transient climate change. *Geophys. Res. Lett.*, **33**, L17704, doi:10.1029/2006GL027242.

- Taylor, K. E., R. J. Stouffer, and G. A. Meehl, 2012: An overview of CMIP5 and the experiment design. *Bull. Amer. Meteor. Soc.*, **93**, 485–498, doi:[10.1175/BAMS-D-11-00094.1](https://doi.org/10.1175/BAMS-D-11-00094.1).
- Trossman, D. S., J. B. Palter, T. M. Merlis, Y. Huang, and Y. Xia, 2016: Large-scale ocean circulation-cloud interactions reduce the pace of transient climate change. *Geophys. Res. Lett.*, **43**, 3935–3943, doi:[10.1002/2016GL067931](https://doi.org/10.1002/2016GL067931).
- Vecchi, G. A., and Coauthors, 2014: On the seasonal forecasting of regional tropical cyclone activity. *J. Climate*, **27**, 7994–8016, doi:[10.1175/JCLI-D-14-00158.1](https://doi.org/10.1175/JCLI-D-14-00158.1).
- Weaver, A. J., M. Eby, M. Kienast, and O. A. Saenko, 2007: Response of the Atlantic meridional overturning circulation to increasing atmospheric CO<sub>2</sub>: Sensitivity to mean climate state. *Geophys. Res. Lett.*, **34**, L05708, doi:[10.1029/2006GL028756](https://doi.org/10.1029/2006GL028756).
- Winton, M., 2003: On the climatic impact of ocean circulation. *J. Climate*, **16**, 2875–2889, doi:[10.1175/1520-0442\(2003\)016<2875:OTCIOO>2.0.CO;2](https://doi.org/10.1175/1520-0442(2003)016<2875:OTCIOO>2.0.CO;2).
- , K. Takahashi, and I. M. Held, 2010: Importance of ocean heat uptake efficacy to transient climate change. *J. Climate*, **23**, 2333–2344, doi:[10.1175/2009JCLI3139.1](https://doi.org/10.1175/2009JCLI3139.1).
- , S. M. Griffies, B. L. Samuels, J. L. Sarmiento, and T. L. Frölicher, 2013: Connecting changing ocean circulation with changing climate. *J. Climate*, **26**, 2268–2278, doi:[10.1175/JCLI-D-12-00296.1](https://doi.org/10.1175/JCLI-D-12-00296.1).
- , W. G. Anderson, T. L. Delworth, S. M. Griffies, W. J. Hurlin, and A. Rosati, 2014: Has coarse ocean resolution biased simulations of transient climate sensitivity? *Geophys. Res. Lett.*, **41**, 8522–8529, doi:[10.1002/2014GL061523](https://doi.org/10.1002/2014GL061523).
- Xie, P., and G. K. Vallis, 2012: The passive and active nature of ocean heat uptake in idealized climate change experiments. *Climate Dyn.*, **38**, 667–684, doi:[10.1007/s00382-011-1063-8](https://doi.org/10.1007/s00382-011-1063-8).
- Zhang, R., S. M. Kang, and I. M. Held, 2010: Sensitivity of climate change induced by the weakening of the Atlantic meridional overturning circulation to cloud feedback. *J. Climate*, **23**, 378–389, doi:[10.1175/2009JCLI3118.1](https://doi.org/10.1175/2009JCLI3118.1).
- Zhang, S., M. J. Harrison, A. Rosati, and A. Wittenberg, 2007: System design and evaluation of coupled ensemble data assimilation for global oceanic climate studies. *Mon. Wea. Rev.*, **135**, 3541–3564, doi:[10.1175/MWR3466.1](https://doi.org/10.1175/MWR3466.1).